7-27-2010

Synthesis of satellite (MODIS), aircraft (ICARTT), and surface (IMPROVE, EPA-AQS, AERONET) aerosol observations over eastern North America to improve MODIS aerosol retrievals and constrain surface aerosol concentrations and sources

Easan Drury
Harvard University

Daniel J. Jacob
Harvard University

Robert J.D. Spurr
RT Solutions, Inc.

Jun Wang
University of Nebraska - Lincoln

Yohei Shinozuka
NASA

See next page for additional authors

Authors

Easan Drury, Daniel J. Jacob, Robert J.D. Spurr, Jun Wang, Yohei Shinozuka, Bruce E. Anderson, A D. Clarke, Jack E. Dibb, Cameron McNaughton, and Rodney J. Weber

Synthesis of satellite (MODIS), aircraft (ICARTT), and surface (IMPROVE, EPA-AQS, AERONET) aerosol observations over eastern North America to improve MODIS aerosol retrievals and constrain surface aerosol concentrations and sources

Easan Drury,[1,2] Daniel J. Jacob,[1] Robert J. D. Spurr,[3] Jun Wang,[4] Yohei Shinozuka,[5] Bruce E. Anderson,[6] Antony D. Clarke,[7] Jack Dibb,[8] Cameron McNaughton,[7] and Rodney Weber[9]

[1] We use an ensemble of satellite (MODIS), aircraft, and ground-based aerosol observations during the ICARTT field campaign over eastern North America in summer 2004 to (1) examine the consistency between different aerosol measurements, (2) evaluate a new retrieval of aerosol optical depths (AODs) and inferred surface aerosol concentrations (PM$_{2.5}$) from the MODIS satellite instrument, and (3) apply this collective information to improve our understanding of aerosol sources. The GEOS-Chem global chemical transport model (CTM) provides a transfer platform between the different data sets, allowing us to evaluate the consistency between different aerosol parameters observed at different times and locations. We use an improved MODIS AOD retrieval based on locally derived visible surface reflectances and aerosol properties calculated from GEOS-Chem. Use of GEOS-Chem aerosol optical properties in the MODIS retrieval not only results in an improved AOD product but also allows quantitative evaluation of model aerosol mass from the comparison of simulated and observed AODs. The aircraft measurements show narrower aerosol size distributions than those usually assumed in models, and this has important implications for AOD retrievals. Our MODIS AOD retrieval compares well to the ground-based AERONET data ($R = 0.84$, slope = 1.02), significantly improving on the MODIS c005 operational product. Inference of surface PM$_{2.5}$ from our MODIS AOD retrieval shows good correlation to the EPA-AQS data ($R = 0.78$) but a high regression slope (slope = 1.48). The high slope is seen in all AOD-inferred PM$_{2.5}$ concentrations (AERONET: slope = 2.04; MODIS c005: slope = 1.51) and could reflect a clear-sky bias in the AOD observations. The ensemble of MODIS, aircraft, and surface data are consistent in pointing to a model overestimate of sulfate in the mid-Atlantic and an underestimate of organic and dust aerosol in the southeastern United States. The sulfate overestimate could reflect an excessive contribution from aqueous-phase production in clouds, while the organic carbon underestimate could possibly be resolved by a new secondary pathway involving dicarbonyls.

[1]School of Engineering and Applied Sciences, Harvard University, Cambridge, Massachusetts, USA.
[2]National Renewable Energy Laboratory, Golden, Colorado, USA.
[3]RT Solutions, Inc., Cambridge, Massachusetts, USA.
[4]Department of Geosciences, University of Nebraska, Lincoln, Nebraska, USA.

[5]NASA Ames Research Center, Moffett Field, California, USA.
[6]NASA Langley Research Center, Hampton, Virginia, USA.
[7]School of Ocean and Earth Science and Technology, University of Hawaii, Manoa, Hawaii, USA.
[8]Institute for the Study of Earth, Oceans, and Space, University of New Hampshire, Durham, New Hampshire, USA.
[9]School of Earth and Atmospheric Sciences, Georgia Institute of Technology, Atlanta, Georgia, USA.

1. Introduction

[2] Measuring atmospheric aerosol concentrations is of considerable interest for a wide range of environmental issues ranging from public health to climate change. Ground-based measurements have sparse geographical coverage, while aircraft measurements have sparse temporal coverage. Satellite remote sensing provides global continuous coverage, but accurate quantitative retrieval of aerosol properties from the measured radiances is a major challenge. In this paper, we use a new algorithm to retrieve aerosol optical depths (AODs) from the MODIS satellite instrument [*Drury et al.*, 2008] and apply it to North America for the summer 2004 period of the ICARTT aircraft field campaigns. We use the satellite, aircraft, and ground-based aerosol observations over this period, in combination with a global three-dimensional chemical transport model (GEOS-Chem CTM), to test the consistency of this integrated aerosol observing system and improve our understanding of U. S. aerosol sources.

[3] The MODIS instruments on board the Terra and Aqua platforms have been used extensively for global mapping of AODs [*Remer et al.*, 2006; *Levy et al.*, 2007a]. MODIS measures backscattered solar radiation with seven wavelength bands dedicated to aerosol retrieval (0.47, 0.55, 0.65, 0.85, 1.24, 1.65, and 2.13 μm). The instrument has a nadir resolution of 250–500 m and a cross-track nadir swath of 2330 km, providing global coverage every 1–2 days at 1030 local time (Terra) and 1330 local time (Aqua) [*Kaufman et al.*, 1997]. AODs have been retrieved operationally from the measured top-of-atmosphere (TOA) reflectances at 10×10 km^2 resolution since February 2000 (Terra) and August 2002 (Aqua) [*Chu et al.*, 2002; *Remer et al.*, 2005, 2006]. MODIS AODs are most reliable over the ocean [*Remer et al.*, 2002; *Levy et al.*, 2005], while the data over land have been subject to higher uncertainty and a persistent high bias [*Ichoku et al.*, 2002; *Kinne et al.*, 2003; *Chin et al.*, 2004; *Levy et al.*, 2005]. The most recent collection 5 MODIS land AOD shows significant improvement over the collection 4 product [*Levy et al.*, 2007a], but it is still biased high over arid regions in the southwestern United States [*Drury et al.*, 2008].

[4] The quality of MODIS AOD data depends on the ability to (1) distinguish atmospheric reflectance from surface reflectance and (2) relate atmospheric reflectance to AOD. The collection 5 MODIS AOD retrieval estimates 0.47 and 0.65 μm land surface reflectances by using the TOA reflectance at 2.13 μm (where the atmosphere is near-transparent), the Sun/satellite measurement geometry, and the local normalized difference vegetation index (NDVI). Measurement geometry and NDVI are used to calculate a 0.65:2.13 surface reflectance ratio for each scene, and the 0.47:0.65 surface reflectance relationship is specified by a slope of 0.49 plus an intercept of 0.005 [*Remer et al.*, 2006; *Levy et al.* 2007a]. AODs are then retrieved from the residual atmospheric reflectances by assuming that aerosol optical properties are known. The collection 5 MODIS AOD algorithm assumes fixed aerosol optical properties for individual continental regions and seasons based on available climatological data [*Remer et al.*, 2006; *Levy et al.* 2007b].

[5] In a preceding paper, we developed a new method for using MODIS TOA reflectances to infer AODs [*Drury et al.*, 2008]. The method characterizes visible surface reflectance from locally derived 0.47:2.13 and 0.65:2.13 μm surface reflectance ratios calculated from subsets of MODIS observations corresponding to low-aerosol conditions. AODs are then retrieved from the residual aerosol reflectances using local aerosol composition data taken from a global chemical transport model (GEOS-Chem CTM). Evaluation against AOD measurements from the AERONET ground-based network [*Holben et al.*, 2001] during the ICARTT period showed considerable improvement over the operational MODIS AOD products in the western and central United States. However, we still had a low AOD bias in the eastern United States. In the present work, we understand and correct this bias by using the in situ aerosol measurements from the ICARTT aircraft.

[6] The International Consortium for Atmospheric Research on Transport and Transformation (ICARTT) brought together several aircraft campaigns (among which NOAA ITCT-2K4 and NASA INTEX-A) operating in eastern North America during the period 6 July to 14 August 2004, in order to quantify regional pollution and continental outflow [*Fehsenfeld et al.*, 2006; *Singh et al.*, 2006]. Aircraft measurements included observations of aerosol mass concentrations, scattering and absorption efficiencies, and size distributions. We focus here mainly on observations from the NASA DC-8 aircraft because of their vertical extent (12 km ceiling), but also reference observations from the NOAA aircraft (which included measurements of organic aerosol, absent from the NASA aircraft). We combine the aircraft data with aerosol observations from surface networks during the ICARTT period including speciated aerosol mass concentrations from the IMPROVE network [*Malm et al.*, 1994], AODs and single scattering albedos (SSAs) from the AERONET network [*Dubovik et al.*, 2000], and mass concentrations of particulate matter of less than 2.5 μm diameter (PM$_{2.5}$) from the U.S. Environmental Protection Agency's Air Quality System (EPA-AQS).

[7] This paper presents a closure analysis, where we examine the consistency of aerosol observations from multiple measurement platforms and use these observations to test our MODIS AOD and PM$_{2.5}$ retrievals. Synthesizing the observations from these different data sets is not a trivial task because of differences in sampling locations, times, and aerosol properties measured. We use the GEOS-Chem CTM as a comparison platform that can bridge across the different observation types and domains and can simulate TOA reflectances to compare with MODIS reflectances [*Drury et al.*, 2008]. GEOS-Chem is driven by our best prior understanding of regional aerosol sources and processes, and we will see how comparison to the ensemble of MODIS and other observations can improve this prior understanding.

2. GEOS-Chem Aerosol Simulation

2.1. General Description

[8] GEOS-Chem is a global CTM driven here by GEOS-4 assimilated meteorological data for 2004 from the NASA Global Modeling and Assimilation Office (GMAO). The GEOS-4 data have $1° \times 1.25°$ horizontal resolution, 36 vertical layers, and a temporal resolution of 6 h (3 h for surface quantities including mixing depths). The model is initialized with a 1 year full chemistry simulation. GEOS-Chem

simulates the mass concentrations of the ensemble of aerosol components during the ICARTT period from 6 July to 14 August, including (1) dust in four size classes, (2) sulfate-nitrate-ammonium (SNA), (3) black carbon (BC), (4) organic carbon (OC), and (5) fine and coarse mode sea salt. We use model version 7-02-04 [http://www-as.harvard.edu/chemistry/trop/geos/index.html] with $2° \times 2.5°$ resolution. A general description of the GEOS-Chem aerosol simulation in the United States is given by *Park et al.* [2004; 2006]. Evaluations of GEOS-Chem aerosol simulations with surface and aircraft observations over the United States have been reported previously for OC [*Park et al.*, 2003; *Heald et al.*, 2006; *van Donkelaar et al.*, 2007; *Fu et al.*, 2009], BC [*Park et al.*, 2003], SNA [*Park et al.*, 2004; *Martin et al.*, 2004], dust [*Fairlie et al.*, 2007], PM$_{2.5}$ [*Liu et al.*, 2005; *van Donkelaar et al.*, 2006], visibility [*Park et al.*, 2006], and AERONET AODs [*Li et al.*, 2005]. The sea-salt simulation has been described and evaluated by *Alexander et al.* [2005].

[9] Aerosol sources and processes used in the present simulation are as described by *Park et al.* [2006], with the addition of dust and sea salt as described by *Fairlie et al.* [2007] and *Alexander et al.* [2005]. Anthropogenic emissions of SO$_2$ and NO$_x$ are from the U.S. EPA National Emissions Inventory (NEI99). Ammonia emissions are from the work of *Bouwmann et al.* [1997], with temperature dependence from the work of *Park et al.* [2004]. Anthropogenic BC emissions are from the work of *Bond et al.* [2004]. The anthropogenic OC emission inventory from the work of *Bond et al.* [2004] underestimates U. S. observations by more than a factor of 2 [*Park et al.*, 2003], and we use instead the emission inventory from the work of *Cooke et al.* [1999], with seasonal adjustments to match IMPROVE data following *Park et al.* [2003]. Secondary organic aerosol (SOA) formation from biogenic terpenes and isoprene is included following *Chung and Seinfeld* [2002] and *Henze and Seinfeld* [2006]. Biofuel emissions are based on the work of *Yevich and Logan* [2003], with seasonal variation from the work of *Park et al.* [2003]. The summer of 2004 was one of the strongest fire seasons on record for Alaska and western Canada, and we use a daily emissions inventory for these fires from the work of *Turquety et al.* [2007], including vertical distribution of injection heights.

2.2. Aerosol Optical Properties

[10] Aerosol optical properties are calculated in GEOS-Chem to determine photolysis rates [*Martin et al.*, 2003] and radiative forcing [*Wang et al.*, 2008] and are used here, following *Drury et al.* [2008], to simulate TOA reflectances for comparison with MODIS measurements. GEOS-Chem aerosol optical properties are calculated by assuming microphysical properties for each aerosol component, with size distributions and refractive indices based on local relative humidity (RH), and using a standard Mie code to generate the wavelength-dependent aerosol extinction efficiencies, SSAs, and scattering phase functions. The local RH values are taken from the GEOS-4 data at the baseline resolution ($1° \times 1.25°$) and show no significant bias relative to values measured from the ICARTT aircraft (Figure 1).

[11] In previous GEOS-Chem studies including the study of *Drury et al.* [2008], aerosol microphysical properties (dry size distributions, hygroscopic growth factors, and refractive indices) were taken from the Global Aerosol Data Set (GADS) [*Koepke et al.*, 1997]. Here we update dry size distributions using measurements from the optical particle counter (OPC) instrument on board the NASA DC-8, as discussed in section 4. Bulk aerosol optical properties are calculated by summing over individual aerosol components to generate a total optical depth, an ensemble SSA, and an ensemble scattering phase function for each vertical model layer. We calculate SSAs by assuming externally mixed aerosol components, which, depending on the local relative humidity and the amount of BC, leads to SSAs that are 2%–5% higher than those for an internally mixed aerosol with a BC core and an SNA or OC shell [*Wang and Martin*, 2007]. Comparisons of observed SSAs to model values assuming either external or internal mixing are presented in section 4.

3. Aerosol Concentrations Measured From Surface and Aircraft

[12] We begin by evaluating the consistency between aircraft, surface, and model concentrations of aerosol components. The NASA DC-8 made 15 flights over eastern North America during the ICARTT campaign, including numerous vertical profiles from 0.3 up to 12 km. We focus attention on measurements over land east of the 100°W meridian. Aerosol mass composition was measured by a particle-into-liquid sampler (PILS) for SNA [*Weber et al.*, 2001] and a combination of filter samples and ion chromatography called SAGA to measure SNA and mineral dust (inferred from Na$^+$ and Ca^{2+}) [*Dibb et al.*, 2003]. BC was measured using a particle soot absorption photometer (PSAP) [*Bond et al.*, 1999]. On the ground, speciated aerosol mass concentrations were measured by the IMPROVE network, comprising 165 field stations located in the wilderness areas of the United States using 24 h filter samples collected every 3 days. The IMPROVE network measures sulfate, nitrate, BC, OC, fine dust mass (diameter < 2.5 μm), and total PM$_{2.5}$ [*Malm et al.*, 1994].

[13] Figure 1 compares the mean observed and modeled vertical profiles of SNA, BC, and dust concentrations during ICARTT. We do not discuss sea-salt concentrations, since they generally constitute a negligible part of the aerosol mass over land. We removed observational outliers defined as values exceeding the mean by more than two standard deviations for each 1 km vertical bin. GEOS-Chem is sampled along the aircraft flight tracks at the time of observation. Mean IMPROVE observations and the corresponding model values are shown by filled squares. We discuss the aerosol components separately in the next paragraphs.

[14] Measured sulfate concentrations from the PILS and SAGA instruments are in good agreement and are consistent with the IMPROVE data. Sulfate is mainly present in the boundary layer below 3 km. Model sulfate mass is 50%–100% higher than the observations. Figure 2 shows the mean horizontal distributions near the surface (0–1 km for the aircraft). The patterns in the aircraft data are noisier than for IMPROVE, and they show spatial differences, but these are also found when the model is applied to each data set (Figure 2, bottom), indicating that they simply reflect sparse temporal sampling by the aircraft. The model bias is mainly in the strong aerosol source regions of the Midwest and
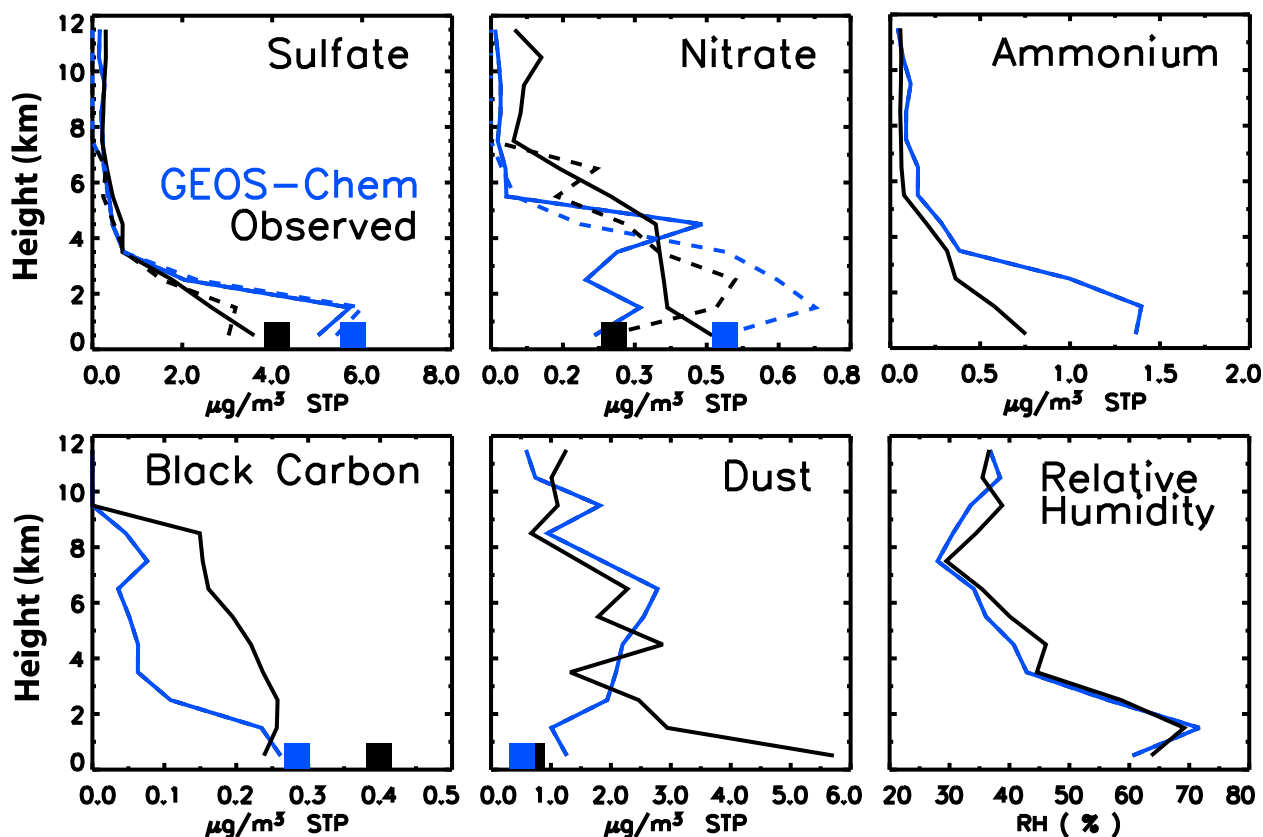
Figure 1. Mean vertical profiles of aerosol mass concentrations and relative humidity over eastern North America (east of 100°W, land only) during ICARTT (6 July to 14 August 2004). DC-8 aircraft observations (black) are compared to model results (blue) sampled along the flight tracks at the time of measurement. For sulfate and nitrate, the dashed and solid lines show measured and model values for the PILS and SAGA instruments, respectively. Measured relative humidity (black) is similarly compared to GEOS-4 assimilated meteorological data (blue). Mean IMPROVE observations are shown by black squares, and the corresponding model values are shown by blue squares. Here and elsewhere, aerosol mass concentrations are in units of $\mu g/m^3$ at standard temperature and pressure (STP).

mid-Atlantic; there is no significant bias outside these source regions. The 1–2 km peak in modeled sulfate (Figure 1) reflects preferential aircraft sampling of sulfate source regions at this altitude. Simulation of ICARTT sulfate observations by an ensemble of regional models found a similar overestimate as that seen here [*McKeen et al.*, 2007], indicating that the bias is not specific to GEOS-Chem.

[15] The model sulfate bias is likely caused by an overestimate of the rate of SO_2 oxidation rather than by an overestimate of SO_2 emission. *Heald et al.* [2006] found no significant bias in comparing GEOS-Chem results for total $SO_x \equiv SO_2$ + sulfate to ICARTT observations. *McKeen et al.* [2007] found that regional models omitting aqueous-phase SO_2 oxidation in clouds did not overestimate sulfate during ICARTT. The good agreement with observations in the periphery of the source regions would appear to reflect the eventual conversion of SO_2 to sulfate.

[16] In a previous GEOS-Chem sulfate simulation for 2001, *Park et al.* [2006] found no significant regional bias compared with IMPROVE observations, and inspection of the IMPROVE data shows no significant decrease from 2001 to 2004. *Park et al.* [2006] used GEOS-3 meteorological data, whereas we used the newer-generation GEOS-4

data set, which has less cloud cover over land. *Koch et al.* [2003] found that sulfate concentrations in source regions are anticorrelated with cloud cover, both in observations and in their model; they attributed this effect to suppression of gas-phase oxidation by OH as well as the correlation of clouds with precipitation. The difference in model results between GEOS-3 and GEOS-4 could thus be driven by cloud cover. However, the lack of bias found by *McKeen et al.* [2007] for the regional models including only gas-phase oxidation of SO_2 suggests that models, in general, may be overestimating the contribution to sulfate from aqueous-phase SO_2 oxidation in clouds. Aqueous-phase oxidation is known to be a major SO_2 sink that needs to be included in models [*Daum et al.*, 1984]. However, *Koch et al.* [2003] found that the standard modeling practice of releasing cloud sulfate in the model grid box at the end of each time step introduces bias by not accounting for the possibility of cloud precipitation at a subsequent time step. They found that tracking the sulfate in cloudy air parcels in their model until the cloud either precipitated or evaporated resulted in a more efficient rainout of sulfate and decreased by 50% of the contribution from aqueous-phase SO_2 oxidation to model sulfate concentrations.
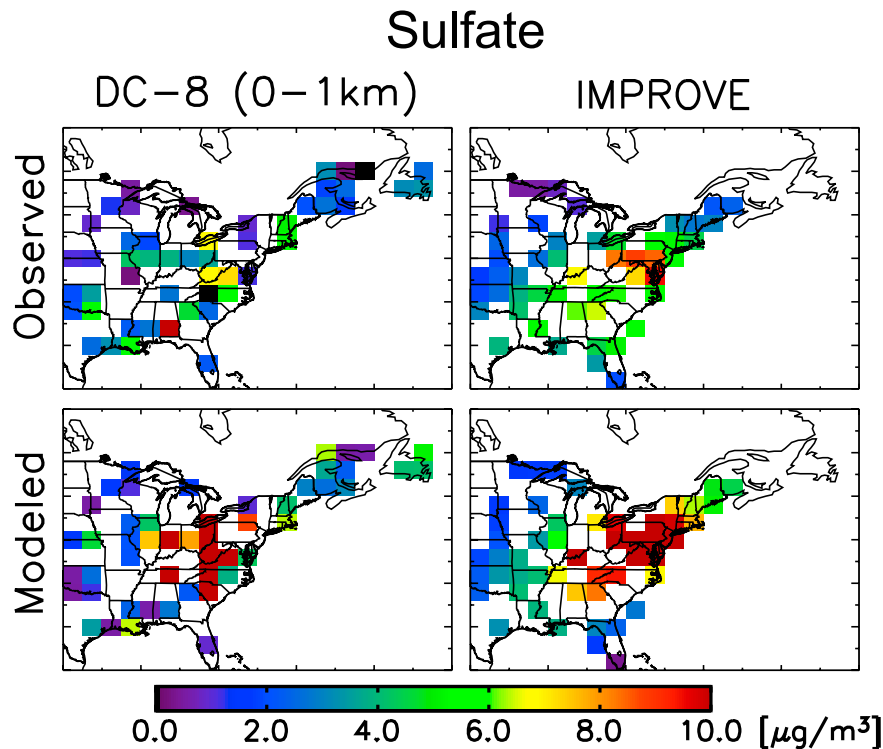
Sulfate

Figure 2. Spatial distribution of near-surface sulfate concentrations measured in eastern North America during ICARTT (6 July to 14 August 2004). (top) Measurements from the aircraft (SAGA instrument, 0–1 km) and at the IMPROVE sites, averaged over the GEOS-Chem 2° × 2.5° grid. (bottom) The GEOS-Chem model values sampled at the time and location of measurements.

[17] Ammonium concentrations measured by the SAGA instrument are lower than model concentrations, with a vertical profile similar to sulfate concentrations. The PILS ammonium measurements suffered from a contamination problem and are not used here. The SAGA data show a regression slope of 0.52 for $[NH_4^+]/(2[SO_4^{2-}] + [NO_3^-])$, implying an acidic ammonium bisulfate aerosol in the mean. The model shows a regression slope of 0.85, similar to previous analysis by *Park et al.* [2004] of CASTNET observations in the eastern United States during the summer of 2001, which found observed and model charge equivalent ratios of 0.79 and 0.84.

[18] Nitrate concentrations in Figure 1 are an order of magnitude lower than sulfate concentrations and contribute a small component to bulk aerosol optical properties. Measurements by PILS, SAGA, and IMPROVE are in fair agreement with each other and with the model simulation.

[19] Black carbon (BC) makes a relatively small contribution to aerosol mass, but it is critical for determining SSAs. We derive the observed mass concentration M_{BC} (g m^{-3}) from aerosol absorption measurements σ_{abs} (m^{-1}) at 550 nm by assuming a mass absorption efficiency β_{abs} (m^2 g^{-1}), following *Chin et al.* [2002]:

$$M_{BC} = \frac{\sigma_{abs}}{\beta_{abs}},\qquad(1)$$

$$\beta_{abs} = (1 - \omega)\frac{3}{4}\frac{Q_\lambda}{\rho r_e}\left(\frac{r_{e,wet}}{r_e}\right)^2,\qquad(2)$$

where ω is the SSA of BC, Q_λ is the quantum extinction efficiency of the wet particle, r_e and $r_{e,wet}$ are the dry and wet effective radii, and ρ is the dry BC density. Using optical properties from GADS, β_{abs} ranges from 7.5 to 14.5 m^2 g^{-1} at 550 nm for relative humidities ranging from 0 to 90%. Since the PSAP filter samples were dried before measuring σ_{abs}, we use β_{abs} = 7.5 m^2 g^{-1}, consistent with previous studies [*Bond and Bergstrom*, 2006; *Thornhill et al.*, 2008].

[20] In addition to the mean vertical profiles in Figure 1, we show in Figure 3 the horizontal distribution of observed and simulated BC mass concentrations. Model BC mass below 1 km is 4% lower than that from PSAP measurements ($R = 0.34$) and 28% lower than that from IMPROVE measurements ($R = 0.44$). These differences are largely due to the southeastern United States, where the high IMPROVE observations (Figure 3) may reflect the sampling of fire events. The 2001 IMPROVE data show low BC concentrations in the Southeast [*Park et al.*, 2006], but in summer 2004 there was a particularly high frequency of fires in the region [*Park et al.*, 2007].

[21] Organic carbon (OC) aerosol concentrations were not measured on the DC-8 aircraft, but water-soluble organic carbon (WSOC) aerosol concentrations were measured on the NOAA P-3 aircraft up to 6 km [*Sullivan et al.*, 2006]. *Heald et al.* [2006] showed that the ICARTT aircraft observations were consistent with the IMPROVE data in the boundary layer and that OC concentrations in the free troposphere were a factor of 2.5 lower than those in the boundary layer after removing transported biomass burning plumes. The relative decrease of OC with height was less
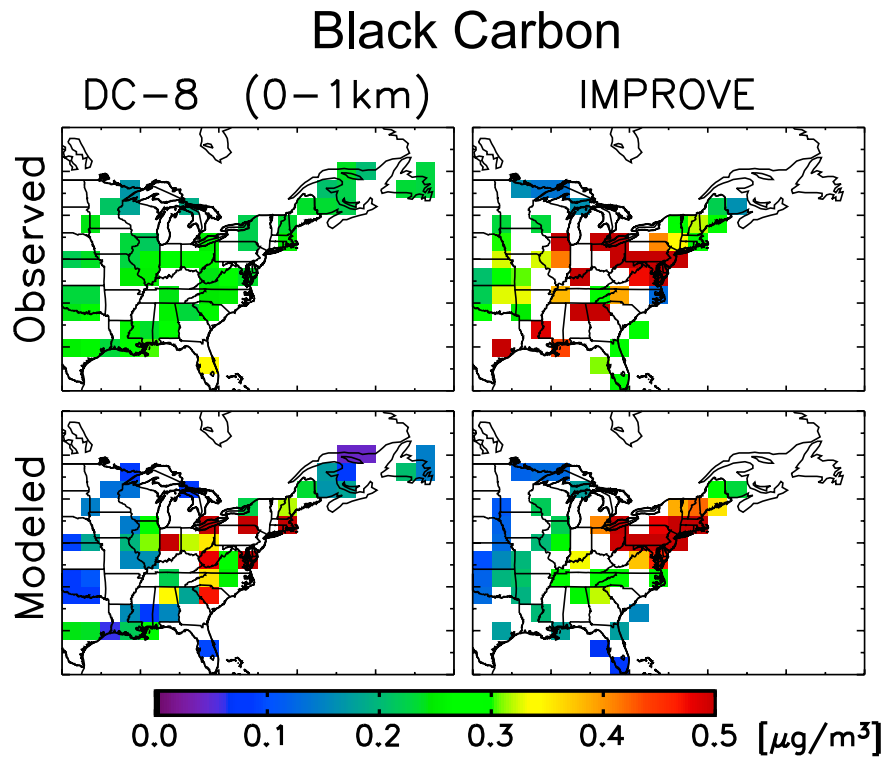
Black Carbon

Figure 3. Same as Figure 2 but for black carbon (BC).

than for sulfate (Figure 1), suggestive of a high-altitude secondary organic aerosol (SOA) source. Previous comparisons of GEOS-Chem OC to aircraft and IMPROVE OC observations during ICARTT were presented by *Heald et al.* [2006] and *Fu et al.* [2009]. *Heald et al.* [2006], using the same version of GEOS-Chem as in the present work, found a 30% underestimate at all altitudes, and similar underestimates were reported in the regional model intercomparison of *McKeen et al.* [2007]. *Fu et al.* [2009] corrected this bias in GEOS-Chem by adding an SOA source from the irreversible uptake of dicarbonyls (glyoxal and methylglyoxal) by cloud droplets, but this additional source is not included here.

[22] Soil dust masses inferred from aircraft ion concentrations near the surface are an order of magnitude higher than those from the IMPROVE data (Figure 1). The instruments have slightly different upper particle size limits (diameters < 2.5 μm for IMPROVE, diameters < 4 μm for the aircraft [*McNaughton et al.*, 2007]), but this is an unlikely explanation for such a large discrepancy. Dust mass is inferred from surface and aircraft observations using different assumptions. IMPROVE dust mass is derived from elemental measurements of Al, Si, Ca, Fe, and Ti by assuming the common oxides, additional mineral compounds, carbonate, and hydrates [*Malm et al.*, 1994] (all concentratuions in μg m^{-3}):

$$[\text{Dust}] = 2.20[\text{Al}] + 2.49[\text{Si}] + 1.63[\text{Ca}] + 2.42[\text{Fe}] + 1.94[\text{Ti}]. \quad (3)$$

Aircraft dust mass is inferred from SAGA Na$^+$ and Ca^{2+} measurements. Na$^+$ is used to isolate the mineral component

of Ca^{2+} from the sea-salt component of Ca^{2+} [*Jordan et al.* 2003], which is defined as:

$$[\text{Ca}^{2+}]_{\text{non-sea salt}} = [\text{Ca}^{2+}] - \frac{0.0439*[\text{Na}^+]}{2}. \quad (4)$$

The remaining Ca^{2+} mass is then used to calculate dust mass using an assumed Ca/dust mass ratio [*Jordan et al.*, 2003; *Fairlie et al.*, 2007]. We calculate a Ca/dust mass ratio of 5.6% for the eastern United States during ICARTT by applying equation (4) to the IMPROVE data, as shown in Figure 4.

[23] One possible cause of the high bias in dust mass inferred from aircraft observations could be anthropogenic emission of Ca^{2+} from industrial processes such as cement manufacturing [*Lee et al.*, 2003; *Sullivan and Prather*, 2005; *Zhang et al.*, 2007]. The dust bias relative to the model is confined to the boundary layer (Figure 1). The IMPROVE data in Figure 5 show a more consistent pattern of uniformly low values, with moderate enhancements in the Southeast from long-range transport of Saharan dust [*Prospero*, 1999]. Model dust concentrations are uniformly low and consistent with IMPROVE observations in the northeast but do not capture the enhancement in the Southeast due to spurious offshore scavenging of the Saharan plume [*Fairlie et al.*, 2007].

[24] Figure 6 shows the mean vertical distribution of total dry aerosol mass concentrations from the model and aircraft observations, using the data from Figure 1 and with the addition of WSOC observations up to 6 km from the PILS instrument aboard the NOAA aircraft. WSOC observations were filtered to remove Alaskan fire plumes following
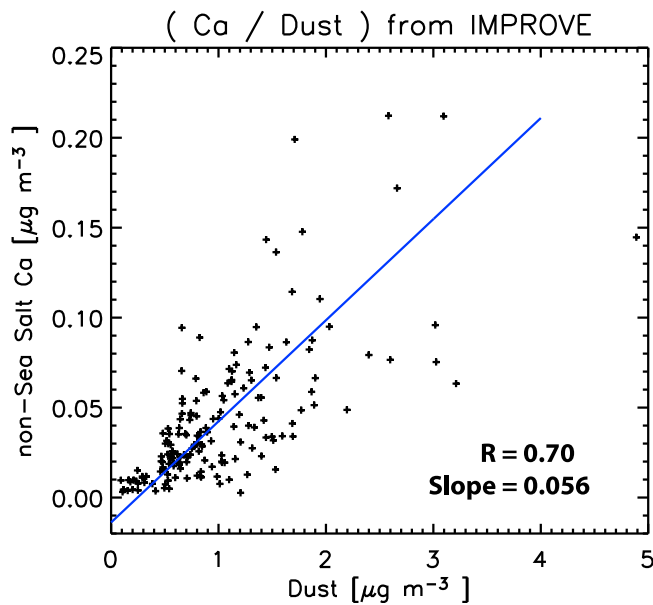
Figure 4. Relationship between non-sea-salt Ca^{2+} and dust mass concentrations measured at IMPROVE surface stations during ICARTT. Non-sea-salt Ca^{2+} is derived from equation (4), and dust concentration is derived from equation (3). The reduced major axis regression line implies a Ca^{2+} mass fraction of 5.6% for dust ($R = 0.70$).

model because of the boundary layer discrepancy discussed above. As we will see, the observed size distributions offer evidence against a large dust contribution in the boundary layer.

4. Aerosol Optical Properties And Optical Depths

[25] Accurately characterizing aerosol microphysical and optical properties is integrally important in retrieving AODs from measured TOA reflectances and in using these AODs (or the observed radiances) to constrain model aerosol mass. The standard assumptions used in GEOS-Chem to calculate aerosol SSAs and size distributions are based on the GADS climatology as described in section 2.2. Here we use surface and aircraft observations during ICARRT to test and improve these assumptions.

[26] We calculate aircraft SSAs from aerosol scattering and absorption measurements. Dry aerosol scattering coefficients were measured at three wavelengths (450, 550, and 700 nm) using an integrating nephelometer instrument [*Anderson et al.*, 1996]. The dry scattering coefficients were corrected for ambient RH using the sensitivity of aerosol scattering to RH measured by two additional nephelometer instruments operating at RH < 40% and RH = 80%, respectively [*Howell et al.*, 2006]. Aerosol absorption was measured by the PSAP instrument after drying the sampled air (RH < 30%), and we use the hygroscopicity of BC from the GADS data base to correct for ambient RH. Column SSAs are also available from the AERONET network based on measurements of diffuse sky radiance [*Dubovik et al.*, 2002]. We use hourly level 2 data, which are cloud screened and quality assured [*Smirnov et al.*, 2000].

Heald et al. [2006]. Total model column aerosol mass agrees with the observations to within 1%, and the vertical distribution is well reproduced. Dust accounts for 41% of column mass in the observations as opposed to 26% in the
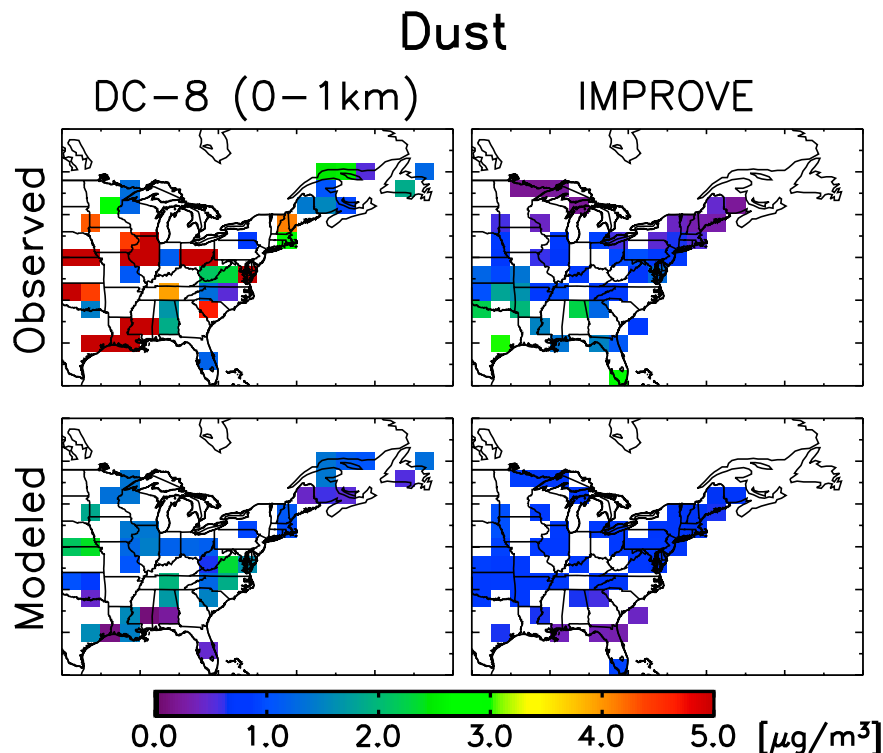
Figure 5. Same as Figure 2 but for dust. We use the model fine dust mass (particle diameter < 2.5 μm) to compare with IMPROVE observations.
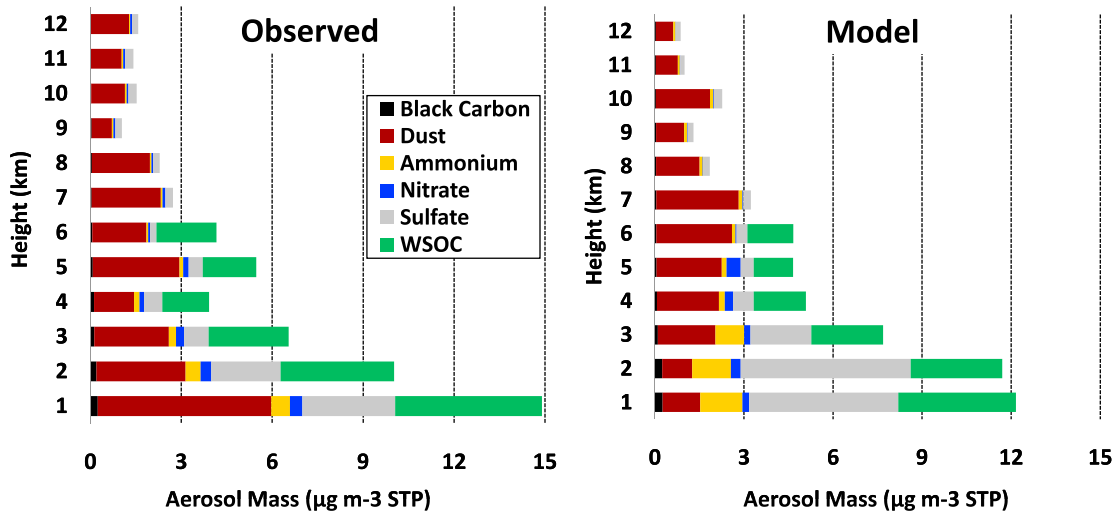
Figure 6. Mean vertical distribution of dry aerosol mass over the eastern United States during ICARTT (6 July to 14 August 2004). Observations from the NASA DC-8 aircraft and from the NOAA P-3 aircraft (water-soluble organic carbon) are compared to model values sampled at the time and location of the aircraft measurements. Sulfate, nitrate, ammonium, and dust are from the SAGA instrument. The WSOC data do not extend above 6 km (NOAA aircraft ceiling).

[27] Figure 7 shows the vertical profile of SSA at 0.47 μm. Model SSAs are calculated by assuming either an externally or internally mixed aerosol, the latter with a BC core and an SNA and OC shell [*Wang and Martin*, 2007]. Dust is externally mixed in both cases. Both the observed and model SSAs decrease with height due to decreasing relative humidity and higher relative BC and dust mass fractions (Figure 6). There is good agreement (within 1%) between the observed SSAs and those modeled with the external mixing assumption below 4 km. Internally mixed model SSAs are 2%–10% lower than observations below 4 km and are in worse agreement with aircraft observations than externally mixed SSAs at all altitudes. In fact, there is certainly some degree of internal mixing in the aerosol, and the better fit of the external mixing parameterization to the aircraft data must reflect weaknesses in the optical model.

[28] Figure 8 compares the geographic distributions of SSAs including column values from the AERONET network. The mean column SSAs measured by aircraft and AERONET are 0.95 and 0.96, and the corresponding model SSAs (externally mixed) are 0.94 and 0.97, respectively. The geographic distributions largely follow those for sulfate (Figure 3). Model SSAs are within 5% of aircraft and AERONET observations everywhere, and the differences would have a minimal impact on our AOD retrieval.

[29] Figure 9 shows the cross-sectional aerosol area size distributions $\left(\frac{dA}{d\log D}\right)$ observed by the Optical Particle Counter (OPC) instrument on board the DC-8 [*Clarke et al.*, 2004, 2007]. These are compared to the model sampled at the times and locations of the measurements. Model cross-sectional area distributions are calculated by summing the lognormal size distributions assumed for each aerosol component [*Seinfeld and Pandis*, 1998]:

$$\frac{dA}{d\log D} = \sum_{i=1}^{n} \frac{\pi D^2}{4} \times \frac{N_i}{\log\sigma_i\sqrt{2\pi}} \exp\left(-\frac{(\log D_{g,i} - \log D)^2}{2\log^2\sigma_i}\right).$$

(5)

In this equation, N_i is the number of aerosol particles of component i per unit volume, $D_{g,i}$ and σ_i are the geometric mean diameter and geometric standard deviation characterizing the lognormal distribution, respectively, and n is the number of aerosol components.

[30] The dashed lines in Figure 9 show the aerosol distributions based on GADS values for the lognormal parameters $D_{g,i}$ and σ_i [*Koepke et al.*, 1997], as used in the standard version of GEOS-Chem [*Martin et al.*, 2003] and tabulated in Table 1. We find that the GADs size parameters do not compare well with OPC observations. In particular, the mode diameters and standard deviations are both too
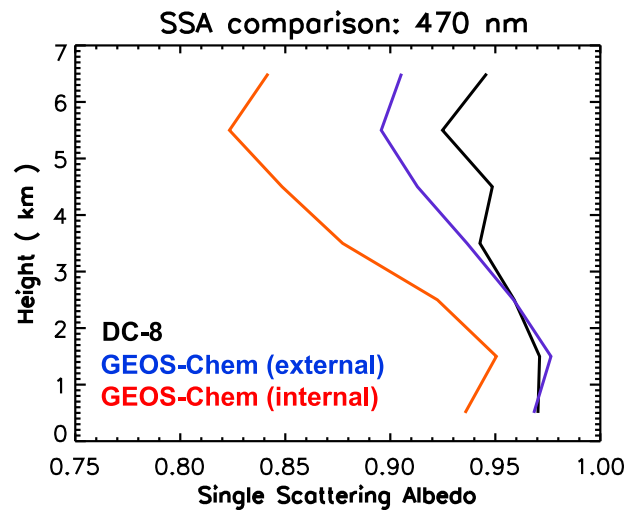

Figure 7. Mean vertical profile of single scattering albedos (SSAs) over the eastern United States during ICARTT (6 July to 14 August 2004). Values measured from the DC-8 aircraft are compared to GEOS-Chem model values assuming either an externally or internally mixed aerosol. The model was sampled at the aircraft locations and times.
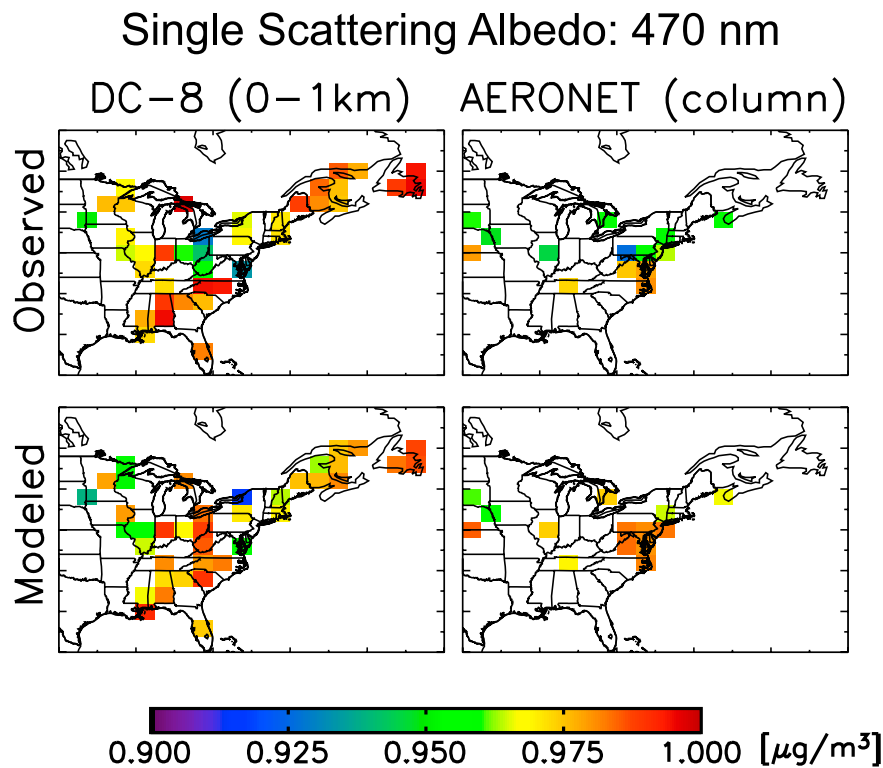
Single Scattering Albedo: 470 nm

Figure 8. Same as Figure 2 but for aerosol single scattering albedo (SSA) with measurements from the DC-8 aircraft and from the AERONET network. Model results assume an externally mixed aerosol and are sampled at the time and location of the measurements.

large. We adjusted these parameters to better fit the OPC measurements, and the results are shown as solid lines. The principal adjustment was to reduce the widths of the log-normal distributions for SNA, OC, and BC from $\sigma = 2.00$–2.20 to $\sigma = 1.60$. The dry SNA geometric mean diameter was held constant at 0.14 μm from GADS, but we increased the dry OC geometric mean diameter from 0.04 to 0.14 μm. We adopted the same geometric mean radius for SNA and OC, since we did not see evidence of multiple accumulation modes in the observations. For BC, we kept the effective diameter constant at 0.08 μm, and the narrower distribution leads to an increased geometric mean diameter of 0.04 from 0.02 μm. For dust, we kept the same $\sigma = 2.20$ for each mode, but we associated a smaller geometric mean diameter from GADS with the model size bins, as shown in Table 1.

[31] The updated aerosol size parameters are consistent with the size parameters inferred from the global AERONET climatology [*Dubovik et al.*, 2002]. Fine-mode urban aerosols were found to have standard deviations of σ in the range 1.46–1.63, while coarse-mode aerosols had values of σ in the range 1.82–2.25. Fine-mode diameters ranged from $D_g = 0.062 - 0.084$ μm for urban and biomass burning aerosols. The observed size distributions in the boundary layer (Figure 9) do not show appreciable aerosol area above 1 μm diameter, further evidence that the dust mass inferred from SAGA observations is biased high.

[32] Our modifications to the aerosol size distributions relative to GADS (in particular, the decreases in σ values) lead to significant differences in model AODs and scattering

phase functions. Model AODs are calculated from the sum of AODs for each aerosol component i as follows:

$$\text{AOD}_\lambda = \sum_{i=1}^{n} \frac{3 M_i Q_{\lambda,i}}{4 \rho_i r_{e,i}}, \qquad (6)$$

where M_i is the mass of aerosol i, $Q_{\lambda,\,i}$ is the quantum extinction efficiency calculated from Mie theory, ρ_i is the aerosol mass density, $r_{e,i}$ is the effective radius which is the ratio of aerosol volume to area based on the aerosol size distribution, and n is the number of aerosol components. Decreasing the spread of the lognormal distribution leads to a larger decrease in $r_{e,i}$ than that for $Q_{\lambda,i}$, and this in turn leads to higher AODs for a given aerosol mass M_i. Table 1 shows the $Q_{\lambda,i}$ and $r_{e,i}$ values calculated using GADS size distributions and our updated size distributions.

[33] Figure 10 compares the mean GEOS-Chem AODs calculated with our improved size distributions versus with GADS. Also shown are the AERONET AOD observations for the ICARTT period. There is a high correlation with AERONET in both cases ($R = 0.87$), but the use of improved size distributions in the model reduces the low model AOD bias relative to AERONET from 21% down to 7%. SSAs calculated using the improved size distributions are only 1%–2% higher than GADS-based values, and this has negligible impact on AOD retrievals.

[34] Aerosol backscattering phase functions are significantly affected by narrowing the aerosol size distributions, and this has a significant impact on the AOD retrieval. Figure 11 plots the ratio of phase functions calculated using
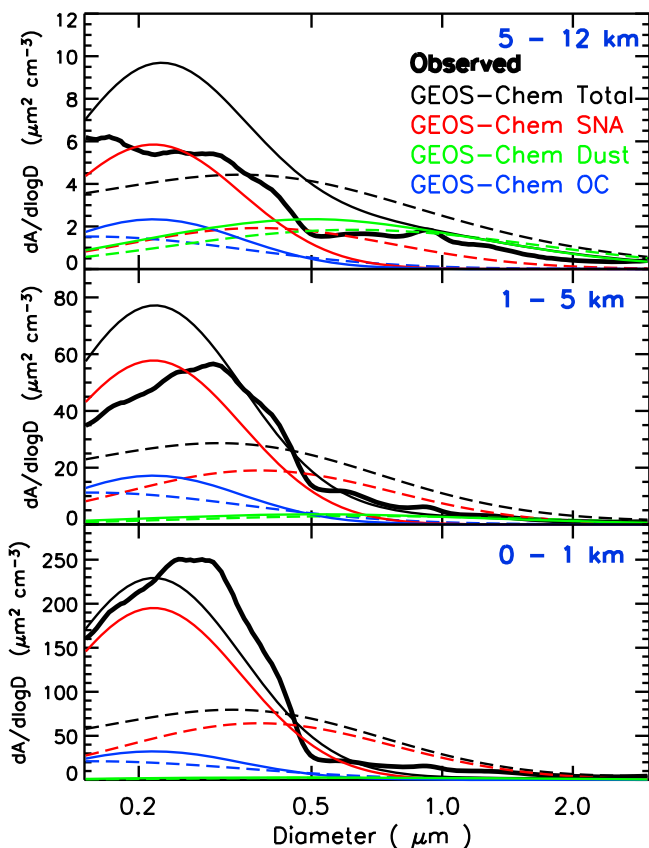
Figure 9. Dry aerosol cross-sectional area size distributions $\left(\frac{dA}{d\log D}\right)$ in different altitude ranges over eastern North America during ICARTT. OPC measurements aboard the DC-8 aircraft (thick black line) are compared to model results sampled at the aircraft locations and times (thin lines). The thin black lines show the simulated aerosol size distribution, and the colored lines show the contributions from the major components (SNA, OC, dust). The dashed lines are for the GADS size distributions, and the solid lines are for the improved size distributions as described in the text.

the improved and the GADS size distributions for the backscatter directions (90°–180°) relevant to AOD retrieval from MODIS. The updated size distributions scatter less light into angles greater than 130° (the prevalent MODIS viewing geometry). The updated size distributions thus lead

to a decrease in model TOA reflectance for a given AOD, which drives the retrieval algorithm to find higher AODs to fit MODIS reflectances.

5. Improved MODIS AOD Retrieval

[35] In *Drury et al.* [2008], we presented an improved MODIS AOD retrieval algorithm including better quantification of surface reflectances and use of local aerosol properties from the GEOS-Chem CTM. The GEOS-Chem evaluation with aircraft and surface concentrations presented in the previous sections and the resulting adjustment of model aerosol optical properties provide us with more confidence in this improved retrieval. Here we describe the retrieval methodology and compare the resulting MODIS AODs with the operational c005 MODIS product and the ground-based AERONET data.

5.1. Methodology

[36] We retrieve AODs from MODIS TOA reflectances following *Drury et al.* [2008] with a few modifications noted below. The retrieval first separates atmospheric reflectance from surface reflectance and then uses model aerosol optical properties to relate atmospheric reflectances to AODs using a radiative transfer code. The visible surface reflectance is estimated for each MODIS scene based on locally derived 0.47:2.13 and 0.65:2.13 μm surface reflectance ratios under clean weather conditions when aerosol reflectance is minimum. These ratios are calculated for the ICARTT time period (6 July to 14 August 2004) by collecting all of the cloud-screened 10×10 km^2 MODIS reflectance data for each $1° \times 1.25°$ horizontal scene and taking the lower envelope of a plot of 0.47 versus 2.13 μm (or 0.65 versus 2.13 μm) nadir-scaled TOA reflectances [*Drury et al.*, 2008].

[37] These surface reflectances at 0.47 and 0.65 μm, together with the local GEOS-Chem aerosol optical properties, are then used to simulate TOA reflectances in the MODIS viewing geometry using the LIDORT multiple scattering radiative transfer model [*Spurr*, 2002]. Model AODs are iteratively scaled until the simulated TOA reflectances match observed MODIS reflectances, and this represents our MODIS AOD product. Further details on the method are given by *Drury et al.* [2008]. Aside from any advantage gained from the use of local CTM aerosol optical properties as opposed to mean climatological values to

Table 1. Aerosol Size and Optical Properties[a]

| Aerosol | GADS[b] | | | | This Study | | | |
	D_{mode} (μm)	σ	D_{eff} (μm)	Q_{ext}	D_{mode} (μm)	σ	D_{eff} (μm)	Q_{ext}
Sulfate-Nitrate-Ammonium	0.20	2.00	0.69	2.25	0.20	1.60	0.34	1.29
Organic Carbon	0.05	2.24	0.27	1.03	0.17	1.60	0.30	1.34
Black Carbon	0.02	2.00	0.08	0.62	0.04	1.60	0.08	0.59
Dust 1[c]	0.06–0.34	2.20	0.30–1.60	1.44–2.67	0.11	2.20	0.50	2.19
Dust 2	0.53	2.20	2.50	2.45	0.17	2.20	0.80	2.63
Dust 3	1.06	2.20	5.00	2.32	0.34	2.20	1.60	2.67
Dust 4	1.69	2.20	8.00	2.23	0.53	2.20	2.50	2.45

[a]Aerosol size distributions correspond to 50% relative humidity. D_{mode} and D_{eff} are the mode diameter and effective diameter, respectively; σ is the geometric spread of the lognormal distribution, and Q_{ext} is the quantum extinction coefficient calculated at 0.47 μm.
[b]Global Aerosol Data Set (GADS) from the work of *Koepke et al.* [1997] used in the standard version of GEOS-Chem [*Martin et al.*, 2003] and in many climate models.
[c]The smallest model dust size bin represents four modes in the GADS data base, which are aggregated into one [*Chin et al.*, 2002; *Fairlie et al.*, 2007].
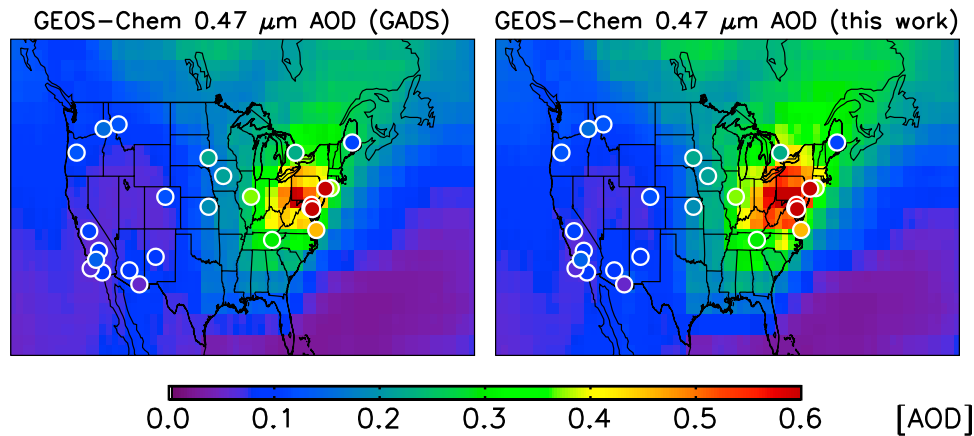
Figure 10. Mean 0.47 μm aerosol optical depths (AODs) over the United States for the ICARTT period (6 July to 14 August 2004). Observations from the AERONET network (circles) are compared to GEOS-Chem model values (background). (left) The GADS size distribution parameters to infer aerosol optical properties from the simulated mass concentrations. (right) Uses the improved parameters derived in this work and given in Table 1. The most important change was to reduce the lognormal geometric standard deviation for fine aerosol from 2.0 to 1.6.

constrain the retrieval, this method ensures that consistent assumptions are used to derive MODIS and GEOS-Chem AODs. This consistency is integrally important in using observed AODs to constrain model aerosol mass in air quality models and in relating aerosol mass to AODs or atmospheric optical properties in climate models.

[38] *Drury et al.* [2008] previously used the above method to retrieve MODIS AODs over the United States during the ICARTT period, and they found a high correlation with AERONET AODs in the western and central United States ($R = 0.90$ at 0.47 μm), with a 19% low bias. However, AODs over the eastern United States were greatly underestimated, particularly for high-aerosol loading events. The AOD retrieval was found to be more accurate at 0.47 than 0.65 μm because of the higher signal-to-noise ratio.

[39] Here we improve the AOD retrieval method in the following manner. First, we alter the SNA, OC, and BC size distributions to match the OPC aircraft measurements, as discussed in section 5. Second, we update the density of black carbon from 1.0 to 1.8 g cm^{-3} following *Bond and Bergstrom* [2006]. Third, we improve our treatment of aerosol scattering phase functions by fitting the Mie output to 32 Legendre polynomials (18 were used previously), and we fit the aerosol forward scattering peaks (0–10° for submicron particles, 0–15° for coarse particles) to exponential forms [*Jacob et al.*, 1989]. This increases the accuracy of the Legendre polynomial fit in the MODIS backscatter directions. Finally, we derive the 0.47:2.13 surface reflectance ratios directly from MODIS TOA reflectances instead of assuming half the value of the 0.65:2.13 ratio (as was done in the c005 MODIS operational retrieval [*Remer et al.*, 2006; *Levy et al.* 2007a] and in the work of *Drury et al.* [2008]). We find 0.47:0.65 ratios greater than 0.5 over urban areas and over eastern Canada.
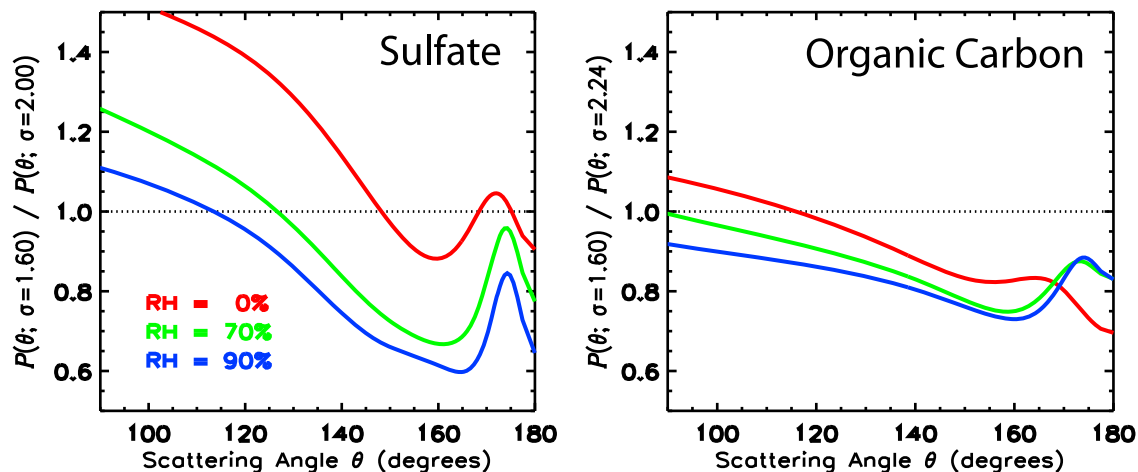

Figure 11. Ratio of the backscattering phase functions $P(\theta)$ for sulfate and OC particles when using improved geometric standard deviations $\sigma = 1.60$ for the lognormal size distributions versus the values used in GADS ($\sigma = 2.0$ for sulfate, $\sigma = 2.24$ for OC). Values are shown for different relative humidities and for backscatter directions from 90° (perpendicular to the incident beam) to 180° (reverse direction).
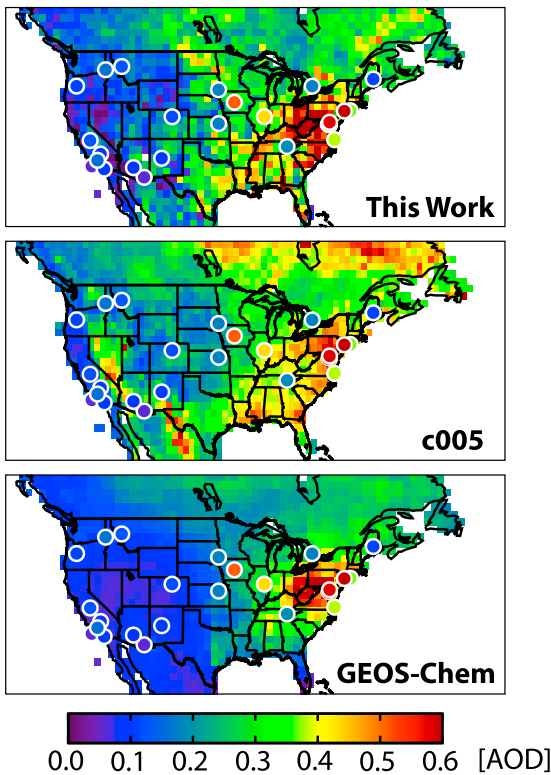
Figure 12. Mean MODIS and GEOS-Chem aerosol optical depths (AODs) at 0.47 μm over North America during ICARTT (6 July to 14 August 2004), with mean AERONET AODs shown as circles. (top) Our MODIS AOD retrieval. (middle) The operational c005 product.

5.2. Application to the ICARTT Period

[40] Figure 12 shows the mean AODs from our MODIS retrieval compared to the operational MODIS c005 AOD product for the ICARTT period. There are significant differences in magnitudes and patterns. To evaluate these differences, we compare in Figure 13 the MODIS and AERONET AOD observations sampled at concurrent times for the ensemble of U.S. AERONET stations (location circles in Figure 12). The comparison uses the temporal average of the concurrent data over the ICARTT period for each site, as limited by MODIS sampling and by cloud cover. We use temporal averages because we have shown previously in the work of *Drury et al.* [2008] that this greatly reduces MODIS noise and that daily comparisons are too noisy to be useful. Results show that the MODIS AODs retrieved with our algorithm are highly correlated with AERONET AODs (R = 0.84), and the associated regression slope implies a small positive bias of 0.05 + 0.02*AOD. The c005 MODIS product shows a similar correlation with AERONET AODs (R = 0.82), but there is a larger and less consistent bias of 0.10–0.21 AOD. It should be noted that the operational MODIS retrieval finds improved performance in its 0.55 μm AOD product, which is designated as the primary retrieval wavelength, even though 0.47, 0.65, and 2.13 μm radiances are used in the retrieval [*Remer et al.*, 2006; *Levy et al.*, 2007a].

[41] Both our improved AOD values and the MODIS operational products show high values over the industrial

Midwest and mid-Atlantic regions, although these are too low in c005 relative to AERONET. Our retrieval and c005 show consistent patterns of elevated AODs in the Southeast that appear to be qualitatively consistent with the fire and dust influences seen in the IMPROVE data (Figure 3). However, there are no AERONET stations in the Southeast to evaluate the retrieval. The relatively high values in the upper Midwest and northeast Canada are consistent with the prevailing transport pathways for the Alaska fire plumes in summer 2004 [*Fuelberg et al.*, 2007; *Turquety et al.*, 2007]. Values over northeast Canada are much higher in c005 than in our retrieval or in the GEOS-Chem model; we find that the 0.47:0.65 surface reflectance ratio in that region is greater than 0.5, suggesting that the MODIS operational retrieval has a high bias. The c005 product also shows spuriously high AODs over arid regions of the southwestern United States due to an underestimate of surface reflectance [*Drury et al.*, 2008]. We also evaluated the MODIS Deep Blue aerosol product [*Hsu et al.*, 2004] but did not find
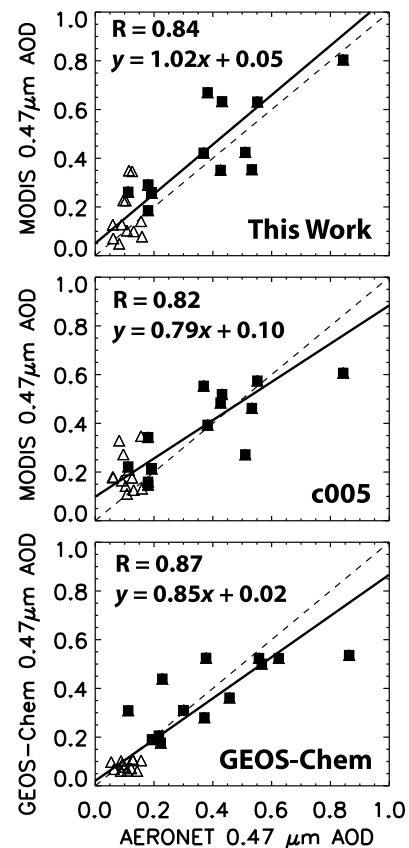

Figure 13. Comparison of mean MODIS and GEOS-Chem aerosol optical depths (AODs) to AERONET observations over North America for the ICARTT period (06 July to 14 August 2004). The MODIS AODs are from our retrieval and from the c005 operational product. Only days with concurrent MODIS and AERONET observations are used in the averaging. Each symbol denotes an AERONET station (squares for east of 100°W, triangles for west of 100°W). Reduced major axis regression statistics are also shown. The regression line is shown as a solid line, and the 1:1 relationship is shown as a dashed line.
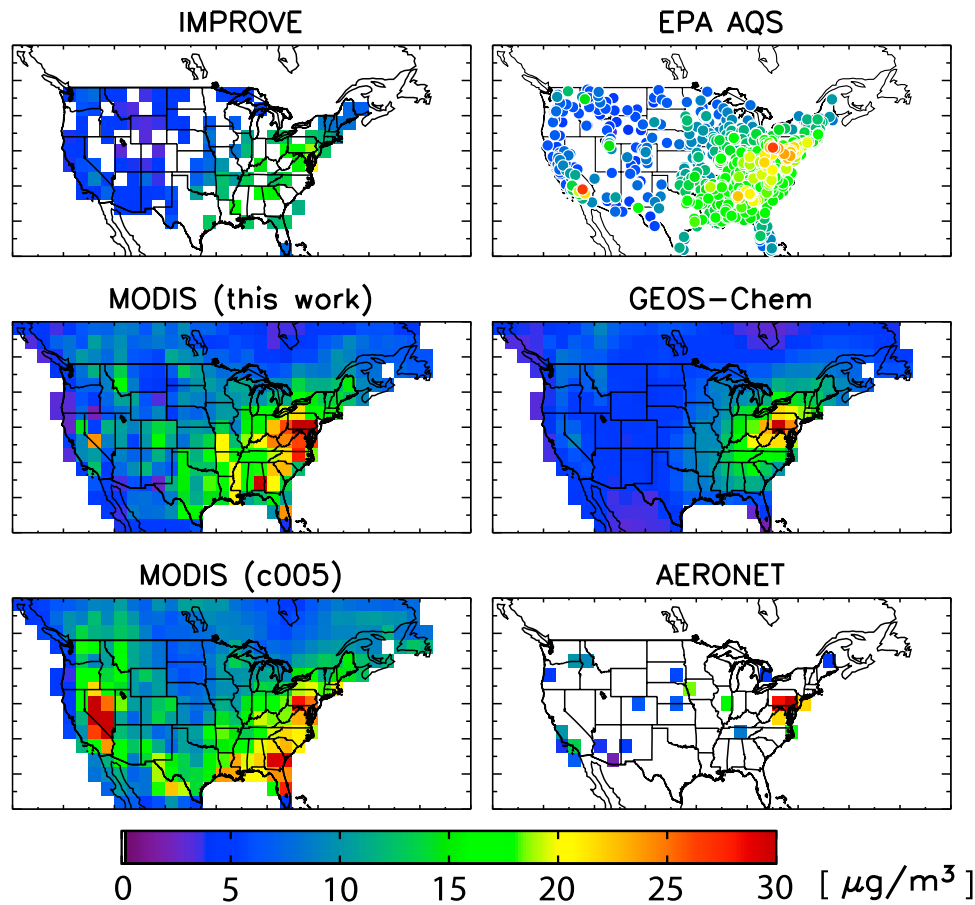
Figure 14. Mean surface PM$_{2.5}$ concentrations over North America during ICARTT (06 July to 14 August 2004). Measurements from IMPROVE and EPA AQS stations are compared to model values (GEOS-Chem) and to values inferred from AODs measured by MODIS (this work), MODIS (c005), and AERONET.

improved performance in the southwestern United States during ICARTT.

[42] The GEOS-Chem AOD simulation is compared to MODIS and AERONET AODs in Figures 10, 12, and 13. In general, it agrees well with AERONET ($R = 0.87$, slope = 0.85). Model AODs are lower than MODIS AODs in the southeastern United States, which is consistent with the previously diagnosed model underestimates of biogenic OC sources [*Heald et al.*, 2006; *van Donkelaar et al.*, 2007] and of transported dust plumes from the Sahara [*Fairlie et al.*, 2007]. The model OC underestimate has since been corrected [*Fu et al.*, 2009], but this correction was not included in our simulation.

6. Inference of Surface PM$_{2.5}$ Concentrations From MODIS AODs

[43] We now examine the potential of our MODIS AOD retrieval to derive surface PM$_{2.5}$ for air quality applications. The bulk of the aerosol column over continental source regions lies in the boundary layer (Figure 6). A number of studies have used AODs measured from space to infer PM$_{2.5}$ [*Wang and Christopher*, 2003; *Liu et al.*, 2005; *van Donkelaar et al.*, 2006; *Shinozuka et al.*, 2007]. The relationship between AODs and PM$_{2.5}$ concentrations can be

constrained empirically from observations for individual sites [*Liu et al.*, 2005] from aircraft observations of aerosol microphysical properties [*Shinozuka et al.*, 2007] or from a CTM simulation [*van Donkelaar et al.*, 2006]. The latter approach has been applied previously using GEOS-Chem [*Liu et al.*, 2005; *van Donkelaar et al.*, 2006]. It is more flexible than the empirical approaches and should be more reliable for spatial extrapolation, but it is contingent on the accuracy of the CTM simulation. Our improved MODIS AOD retrieval, together with our independent evaluation of the GEOS-Chem CTM simulation using both surface and aircraft data, puts us in a favorable position to implement and evaluate this method. We compare the resulting surface PM$_{2.5}$ concentrations with observations from IMPROVE and EPA-AQS stations.

[44] Figure 14 shows the mean 24 h surface PM$_{2.5}$ concentrations measured at IMPROVE and EPA-AQS stations, inferred from MODIS and AERONET AODs, and modeled using GEOS-Chem. PM$_{2.5}$ is inferred from the AOD measurements by scaling with the corresponding GEOS-Chem model ratios [*Liu et al.*, 2005]:

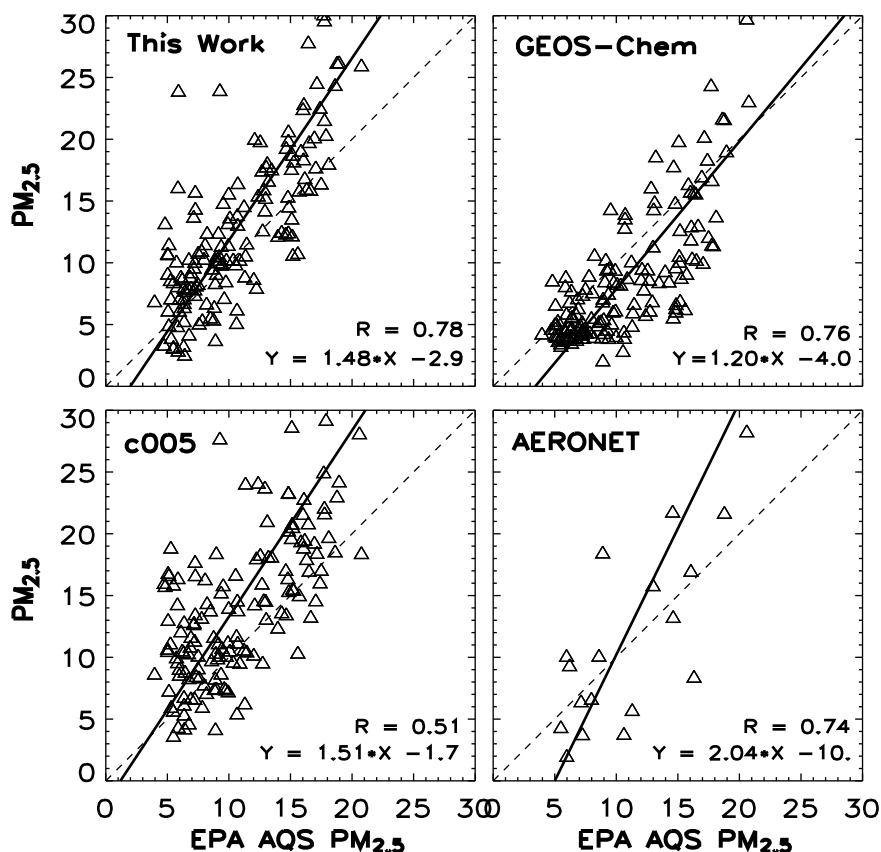$$PM_{2.5} = \left[\frac{PM_{2.5}}{AOD}\right]_{model} AOD, \qquad (7)$$

Figure 15. Comparison of MODIS, GEOS-Chem, and AERONET $PM_{2.5}$ concentrations with mean EPA AQS $PM_{2.5}$ observations averaged over the $2° \times 2.5°$ GEOS-Chem model grid for all stations in North America during the ICARTT period (06 July to 14 August 2004). MODIS $PM_{2.5}$ are from (top left) our retrieval and (bottom left) the c005 operational product. Reduced major axis regression statistics are also shown. The regression line is shown as a solid line, and the 1:1 relationship is shown as a dashed line.

where model $PM_{2.5}$ is a 24 h average and model AOD is sampled at the time of AOD observations. The EPA-AQS stations show higher $PM_{2.5}$ concentrations than the IMPROVE stations, particularly over strong aerosol source regions, which likely reflects the location of the IMPROVE stations in wilderness areas away from sources. Good general agreement with the EPA-AQS data is found for the $PM_{2.5}$ concentrations simulated by GEOS-Chem and those inferred from our MODIS AOD retrieval or from AERONET AODs following equation (7). In contrast, the $PM_{2.5}$ concentration patterns inferred from the MODIS c005 data depart greatly from the in situ data.

[45] Figure 15 shows the comparison of mean AOD-derived and model $PM_{2.5}$ to EPA-AQS $PM_{2.5}$ observations averaged over the ICARTT period and the $2° \times 2.5°$ model grid. There are many more EPA-AQS stations than AERO-NET stations, and the $PM_{2.5}$ statistics represent different sampling times and locations than the AOD statistics shown in Figure 13. Our retrieval of MODIS $PM_{2.5}$ shows good correlation to the EPA-AQS data ($R = 0.78$) but a high regression slope (1.48). The high slope is seen in all AOD-inferred $PM_{2.5}$ concentrations (AERONET: slope = 2.04; MODIS c005: slope = 1.51) and is caused by an overestimate of $PM_{2.5}$ over strong source regions. This bias could reflect a combination of factors: (1) a clear-sky bias in the remote sensing data, since aerosol concentrations are nega-

tively correlated with cloud cover and precipitation [*Koch et al.*, 2003]; (2) errors in model aerosol vertical profiles, particularly the high-sulfate bias which could contribute too much aerosol mass to the lowest model layers; and (3) a model underestimate of the diurnal variation in surface level $PM_{2.5}$, particularly sulfate. We plan to address these issues in subsequent work.

[46] Figure 16 shows the mean GEOS-Chem model bias for the ICARTT period relative to both our MODIS AOD retrieval and the surface $PM_{2.5}$ from the EPA-AQS network. Both show a model underestimate over the Southeast, due mostly to OC and dust as discussed above. The EPA-AQS data show a large model overestimate over the northeast due to sulfate, as discussed above, but this is not apparent in the AOD data except over New York State. Overall, the results are encouraging for using MODIS AOD data to evaluate model aerosol sources.

7. Conclusions

[47] We used an ensemble of satellite, aircraft, and ground-based aerosol observations during the ICARTT field campaign over eastern North America in summer 2004 to (1) constrain and test a new retrieval of aerosol optical depths (AODs) and inferred surface aerosol ($PM_{2.5}$) concentrations from the MODIS satellite instrument, (2) examine
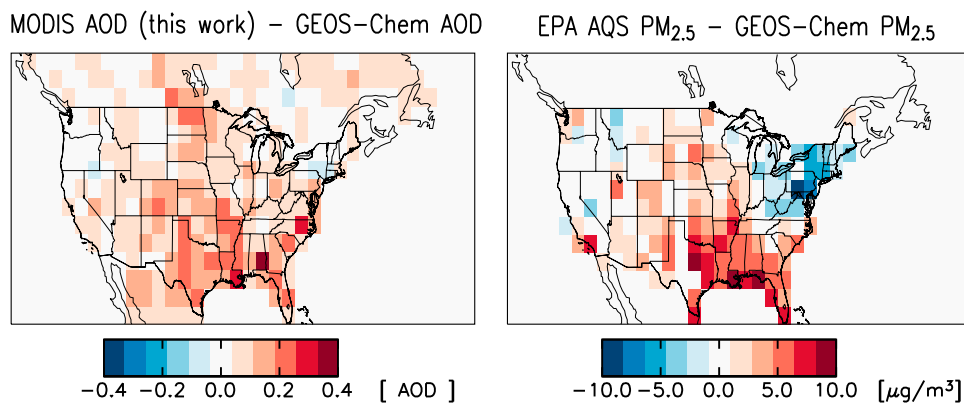
Figure 16. GEOS-Chem model bias relative (left) to our MODIS AOD retrieval and (right) to the EPA-AQS surface PM$_{2.5}$ network. Values are averages for the ICARTT period (06 July to 14 August 2004).

the consistency between different aerosol measurements using the GEOS-Chem chemical transport model (CTM) as an intercomparison platform, and (3) apply this ensemble of information to improve our understanding of aerosol sources in the United States. Our MODIS AOD retrieval uses a method previously described by *Drury et al.* [2008], which improves on the operational MODIS AOD products by using local visible surface reflectance information derived from low-aerosol scenes as well as aerosol optical properties from the GEOS-Chem model to simulate top-of-atmosphere (TOA) reflectances in the MODIS viewing geometry. We further improve on the *Drury et al.* [2008] retrieval, both in terms of the surface reflectance constraints and in terms of the assumed aerosol optical properties. Aside from any intrinsic advantage in using local aerosol properties from the GEOS-Chem model to constrain the MODIS AOD retrieval, a major benefit is that the model simulation of aerosol mass can then be evaluated from the comparison of simulated and observed AODs.

[48] Comparisons of aerosol chemical data from aircraft, surface sites, and the GEOS-Chem model during the ICARTT campaign show various degrees of consistency. The aerosol mass is dominated by sulfate, organic carbon (OC), and dust. Aerosol absorption is dominated by black carbon (BC). The dust measurements aboard the aircraft show high concentrations in the boundary layer, but this appears inconsistent with the rest of the data. The model tends to overestimate sulfate over source regions and underestimate OC and BC aerosol over the Southeast. The OC underestimate could be corrected by including in the model an additional source from dicarbonyls [*Fu et al.*, 2009]. The BC simulation compares well with observed BC concentrations from previous years (2001–2003 [*Park et al.*, 2007]) but does not capture additional fire activity in the summer of 2004. Fire and dust plumes transported over the eastern United States increase aerosol absorptivity in the free troposphere.

[49] The aircraft data include vertical profiles up to 12 km of aerosol single-scattering albedos (SSAs) and size distributions to help constrain the MODIS AOD retrieval. Observed SSAs decrease slightly from 0.97 in the boundary layer to 0.94 in the upper troposphere, reflecting an increase in BC mass fractions with altitude. Model SSAs are consistent with the aircraft profiles under the assumption of an

external aerosol mixture and are also then in good agreement with the column SSAs measured by the ground-based AERONET network. Comparisons of simulated and observed aerosol size distributions show that the commonly used lognormal size distributions for individual aerosol components from the Global Aerosol Data Set (GADS) [*Koepke et al.*, 1997] are too broad. Use of narrower size distributions in the model (geometric standard deviation $\sigma = 1.6$ for the fine components) improves the fit to the aircraft data and also removes the prior bias in comparing model AODs to AERONET observations. This has important implications for the MODIS retrieval, as the updated model size distributions result in significantly higher AODs for a given TOA reflectance.

[50] We compared our MODIS AOD retrieval for the ICARTT period to the c005 MODIS operational AOD product and to the well-calibrated standard offered by AERONET AODs. Our MODIS AOD retrieval shows significant differences with the MODIS operational product, both in the magnitude and distribution of AODs, and is in better general agreement with the AERONET data ($R = 0.84$, bias 0.05 + 0.02*AOD). In particular, our retrieval resolves the problem of anomalously high AODs over the arid Southwest in the operational product.

[51] It shows high values in areas of the southeastern United States that are not found in GEOS-Chem and likely reflect the regional model underestimate of OC sources from vegetation and fires.

[52] We used our MODIS AOD retrieval to infer surface concentrations of fine particulate matter (PM$_{2.5}$) by scaling to the local AOD/PM$_{2.5}$ ratio from GEOS-Chem and taking advantage of the prior validation of that ratio by the aircraft observations. Comparison to the dense network of EPA-AQS monitoring stations shows a high degree of consistency, demonstrating the value of the MODIS data for mapping PM$_{2.5}$ air quality. The inferred MODIS PM$_{2.5}$ concentrations tend to be higher than observations in source regions, as are all AOD-derived PM$_{2.5}$ concentrations, and this could reflect the clear-sky bias of AOD observations.

[53] Our MODIS AOD retrieval algorithm was applied here to the summertime United States because of a unique ensemble of aerosol data available for testing, but it can easily be applied to other geographic regions and seasons. Local surface reflectances can be determined from the

subset of low-aerosol scenes diagnosed by low visible reflectance; this does not assume that the aerosol contribution to reflectance is negligible, only that the visible/infrared reflectance ratio is determined by the surface and that the ratio remains constant during the period of interest. Local aerosol properties can be specified from any CTM simulation. Results will be sensitive to the aerosol size distribution and single-scattering albedo, so an independent check on the quality of the CTM simulation for these quantities is valuable. Our MODIS AOD algorithm is currently being applied in multiyear studies over China and North America, and the results of these analyses will be presented in forthcoming publications.

References

Alexander, B., J. Savarino, C. C. W. Lee, R. J. Park, D. J. Jacob, M. H. Thiemens, Q. B. Li, and R. M. Yantosca (2005), Sulfate formation in sea-salt aerosols: Constraints from oxygen isotopes, *J. Geophys. Res.*, *110*(D10), D10307, doi:10.1029/2004JD005659.

Anderson, T. L., et al. (1996), Performance characteristics of a high-sensitivity, three-wavelength, total scatter/backscatter nephelometer, *J. Atmos. Oceanic Technol.*, *13*, 967–986.

Bond, T. C., and R. W. Bergstrom (2006), Light absorption by carbonaceous particles: An investigative review, *Aerosol Sci. Technol.*, *39*, 1–41.

Bond, T. C., T. L. Anderson, and D. Campbell (1999), Calibration and intercomparison of filter-based measurements of visible light absorption by aerosols, *Aerosol Sci. Technol.*, *30*, 582–600.

Bond, T. C., D. G. Streets, K. F. Yarbar, S. M. Nelson, J. H. Woo, and Z. Klimont (2004), A technology-based global inventory of black and organic carbon emissions from combustion, *J. Geophys. Res.*, *109*(D14), D14203, doi:10.1029/2003JD003697.

Bouwmann, A. F., D. S. Lee, W. A. H. Asman, F. J. Dentener, K. W. VanderHoek, and J. G. J. Olivier (1997), A global high-resolution emission inventory for ammonia, *Global Biogeochem. Cycles*, *11*(4), 561–587.

Chin, M., P. Ginoux, S. Kinne, O. Torres, B. N. Holben, B. N. Duncan, R. V. Martin, J. A. Logan, A. Higurashi, T. Nakajima (2002), Tropospheric aerosol optical thickness from the GOCART model and comparisons with satellite and sun photometer measurements, *J. Atmos. Sci.*, *59*, 461–483.

Chin, M., A. Chu, R. Levy, L. Remer, Y. Kaufman, B. Holben, T. Eck, P. Ginoux, and Q. Gao (2004), Aerosol distribution in the Northern Hemisphere during ACE-Asia: Results from global model, satellite observations, and Sun photometer measurements, *J. Geophys. Res.*, *109*(D23), D23S90, doi:10.1029/2004JD004829.

Chu, D. A., Y. J. Kaufman, C. Ichoku, L. A. Remer, D. Tanre, and B. N. Holben (2002), Validation of MODIS aerosol optical depth retrieval over land, *Geophys. Res. Lett.*, *29*(12), 8007, doi:10.1029/2001GL013205.

Chung, S. H., and J. H Seinfeld (2002), Global distribution and climate forcing of carbonaceous aerosols, *J. Geophys. Res.*, *107*(D19), 4407, doi:10.1029/2001JD001397.

Clarke, A. D., et al. (2004), Size distributions and mixtures of dust and black carbon aerosol in Asian outflow: Physiochemistry and optical properties, *J. Geophys. Res.*, *109*(D15), D15S09, doi:10.1029/2003JD004378.

Clarke, A., C. McNaughton, B. Kapustin, Y. Shinozuka, S. Howell, J. Dibb, J. Zhou, B. Anderson, V. Brekhovskikh, and M. Pinkerton (2007), Biomass burning and pollution aerosol over North America: Organic components and their influence on spectral optical properties and humidification response, *J. Geophys. Res.*, *112*(D12), D12S18, doi:10.1029/2006JD007777.

Cooke, W. F., C. Liousse, H. Cachier, and J. Feichter (1999), Construction of a 1 × 1 fossil fuel emission data set for carbonaceous aerosol and implementation and radiative impact in the ECHAM-4 model, *J. Geophys. Res.*, *104*(D18), 22,137–22,162.

Daum, P. H., T. J. Kelly, S. E. Schwartz, and L. Newman (1984), Measurements of the chemical composition of stratiform clouds, *Atmos. Environ.*, *18*(12), 2671–2684.

Dibb, J. E., R. W. Talbot, E. M. Scheuer, D. R. Blake, N. J. Blake, G. L. Gregory, G. W. Sachse, and D. C. Thornton (1999), Aerosol chemical composition and distribution during the Pacific Exploratory Mission (PEM) Tropics, *J. Geophys. Res.*, *104*(D5), 5785–5800.

Dibb, J. E., R. W. Talbon, E. M. Scheuer, G. Seid, M. A. Avery, and H. B. Singh (2003), Aerosol chemical composition in Asian continental outflow during the TRACE-P campaign: Comparison with PEM West B, *J. Geophys. Res.*, *108*(D21), 8815, doi:10.1029/2002JD003111.

Drury, E. E., D. J. Jacob, J. Wang, R. J. D. Spurr, and K. V. Chance (2008), Improved algorithm for MODIS satellite retrievals of aerosol optical depths over western North America, *J. Geophys. Res.*, *113*(D16), D16204, doi:10.1029/2007JD009573.

Dubovik, O., A. Smirnov, B. N. Holben, M. D. King, Y. J. Kaufman, T. F. Eck, and I. Slutsker (2000), Accuracy assessment of aerosol optical properties retrieval from the sky radiance and solar transmittance measured from ground, *J. Geophys. Res.*, *103*(31), 903–924.

Dubovik, O., B. Holben, T. F. Eck, A. Smirnov, Y. J. Kaufman, M. D. King, D. Tanre, and I. Slutsker (2002), Variability of absorption and optical properties of key aerosol types observed in worldwide locations, *J. Atmos. Sci.*, *59*, 590–608.

Fairlie, T. D., D. J. Jacob, and R. J. Park (2007), The impact of transpacific transport of mineral dust in the United States, *Atmos. Environ.*, *41*, 1251–1266.

Fehsenfeld, F. C., et al. (2006), International Consortium for Atmospheric Research on Transport and Transformation (ICARTT): North America to Europe—Overview of the 2004 summer field study, *J. Geophys. Res.*, *111*(D23), D23S01, doi:10.1029/2006JD007829.

Fu, T. M., D. J. Jacob and C. L. Heald (2009), Aqueous-phase reactive uptake of dicarbonyls as a source of organic aerosol over eastern North America, *Atmos. Environ.*, *43*, 1814–1822.

Fuelberg, H. E., M. J. Porter, C. M. Kiley, J. J. Halland, and D. Morse (2007), Meteorological conditions and anomalies during the Intercontinental Chemical Transport Experiment-North America, *J. Geophys. Res.*, *112*(D12), D12S06, doi:10.1029/2006JD007734.

Heald, C. L., et al. (2006), Concentrations and sources of organic carbon aerosol in the free troposphere over North America, *J. Geophys. Res.*, *111*(D23), D23S47, doi:10.1029/2006JD007705.

Henze, D. K., and J. H. Seinfeld (2006), Global secondary organic aerosol from isoprene oxidation, *Geophys. Res. Lett.*, *33*(9), L09812, doi:10.1029/2006GL025976.

Holben, B. N., et al. (2001), An emerging ground-based aerosol climatology: Aerosol optical depth from AERONET, *J. Geophys. Res.*, *106*(D11), 12,067–12,097.

Howell, S. G., A. D. Clarke, Y. Shinozuka, V. Kapustin, C. S. McNaughton, B. J. Huebert, S. J. Doherty, and T. L. Anderson (2006), Influence of relative humidity upon pollution and dust during ACE-Asia: Size distributions and implications for optical properties, *J. Geophys. Res.*, *111*(D6), D06205, doi:10.1029/2004JD005759.

Hsu, N. C., S. C. Tsay, M. D. King, and J. R. Herman (2004), Aerosol Properties over Bright-Reflecting Source Regions, *IEEE Trans. Geosci. Remote Sens.*, *42*, 557–569.

Ichoku, C., D. A. Chu, S. Mattoo, Y. J. Kaufman, L. A. Remer, D. Tanre, I. Slutsker, and B.N. Holben (2002), A spatio-temporal approach for global validation and analysis of MODIS aerosol products, *Geophys. Res. Lett.*, *29*(12), 8006, doi:10.1029/2001GL013206.

Jacob, D. J., E. W. Gottlieb, and M. J. Prather (1989), Chemistry of a polluted cloudy boundary layer, *J. Geophys. Res.*, *94*(D10), 12,975–13,002.

Jordan, C. E., et al. (2003), Chemical and physical properties of bulk aerosols within four sectors observed during TRACE-P, *J. Geophys. Res.*, *108*(D21), 8813, doi:10.1029/2002JD003337.

Kaufman, Y. J., D. Tanre, H. R. L. A. Remer, E. Vermote, A. Chu, and B. N. Holben (1997), Operational remote sensing of tropospheric aerosol over land from EOS moderate resolution imaging spectroradiometer, *J. Geophys. Res.*, *102*(D14), 17,051–17,067.

Kinne, S., et al. (2003), Monthly averages of aerosol properties: A global comparison among models, satellite data, and AERONET ground data, *J. Geophys. Res.*, *108*(D20), 4634, doi:10.1029/2001JD001253.

Koch, D., J. Park, and A. Del Genio (2003), Clouds and sulfate are anticorrelated: A new diagnostic for global sulfur models, *J. Geophys. Res.*, *108*(D24), 4781, doi:10.1029/2003JD003621.

Koepke, P., M. Hess, I. Schult, and E. P. Shettle (1997), Global Aerosol Data Set, Report No. 243, Max-Planck-Institut fur Meteorologie, Hamburg.

Lee, Y. N., et al. (2003), Airborne measurement of inorganic ionic components of fine aerosol particles using the particle-into-liquid sampler coupled to ion chromatography technique during ACE-Asia and TRACE-P, *J. Geophys. Res.*, *108*(D23), 8646, doi:10.1029/2002JD003265.

Levy, R. C., L. A. Remer, J. V. Martins, Y. J. Kaufman, A. Plana-Fattori, J. Redemann, and B. Wenny (2005), Evaluation of MODIS Aerosol

Retrievals over Ocean and Land during CLAMS, *J. Atmos. Sci.*, *62*, 974–992.

Levy, R. C., L. A. Remer, S. Mattoo, E. F. Vermote, and Y. J. Kaufman (2007a), Second-generation operational algorithm: Retrieval of aerosol properties over land from inversion of Moderate Resolution Imaging Spectroradiometer spectral reflectance, *J. Geophys. Res.*, *112*(D13), D13211, doi:10.1029/2006JD007811.

Levy, R. C., L. A. Remer, and O. Dubovik (2007b), Global aerosol optical properties and application to Moderate Resolution Imaging Spectroradiometer aerosol retrieval over land, *J. Geophys. Res.*, *112*(D13), D13210, doi:10.1029/2006JD007815.

Li, Q., D. J. Jacob, R. Park, Y. Wang, C. L. Heald, R. Hudman, R. M. Yantosca, and R. V. Martin (2005), North American pollution outflow and the trapping of convectively lifted pollution by upper-level anticyclone, *J. Geophys. Res.*, *110*(D10), D10301, doi:10.1029/2004JD005039.

Liu, Y., J. A. Sarnat, V. Kilaru, D. J. Jacob, and P. Koutrakis (2005), Estimating ground-level PM 2.5 in the eastern United States using satellite remote sensing, *Environ. Sci. Technol.*, *39*, 3269–3278.

Malm, W. C., J. F. Sisler, D. Huffman, R. A. Eldred, and T. A. Cahill (1994), Spatial and seasonal trends in particle concentration and optical extinction in the United States, *J. Geophy. Res.*, *99*(D1), 1347–1370.

Martin, R. V., D. J. Jacob, R. M. Yantosca, M. Chin, and P. Ginoux (2003), Global and regional decreases in tropospheric oxidants from photochemical effects of aerosols, *J. Geophys. Res.*, *108*(D3), 4097, doi:10.1029/2002JD002622.

Martin, S. T., H. M. Hung, R. J. Park, D. J. Jacob, R. J. D. Spurr, K. V. Chance, and M. Chin (2004), Effects of the physical state of tropospheric ammonium-sulfate nitrate particles on global aerosol direct radiative forcing, *Atmos. Chem. Phys.*, *4*, 183–214.

McKeen, S., et al. (2007), Evaluation of several PM 2.5 forecast models using data collected during the ICARTT/NEAQS 2004 field study, *J. Geophys. Res.*, *112*(D10), D10S20, doi:10.1029/2006JD007608.

McNaughton, C., et al. (2007), Results from the DC-8 Inlet Characterization Experiment (DICE): Airborne versus surface smpling of mineral dust and sea-salt aerosols, *Aerosol Sci. Technol.*, *41*, 136–159.

Park, R. J., D. J. Jacob, M. Chin, and R. V. Martin (2003), Sources of carbonaceous aerosols over the United States and implications for natural visibility, *J. Geophys. Res.*, *108*(D6), 4355, doi:10.1029/2002JD003190.

Park, R. J., D. J. Jacob, B. D. Field, R. M. Yantosca, and M. Chin (2004), Natural and transboundary pollution influences on sulfate-nitrate-ammonium aerosols in the United States: Implications for policy, *J. Geophys. Res.*, *109*(D15), D15204, doi:10.1029/2003JD004473.

Park, R. J., D. J. Jacob, N. Kumar, and R. M. Yantosca (2006), Regional visibility statistics in the United States: Natural and transboundary pollution influences, and implications for the Regional Haze Rule, *Atmos. Environ.*, *40*, 5405–5423.

Park, R. J., D. J. Jacob, and J. A. Logan (2007), Fire and biofuel contributions to annual mean aerosol mass concentrations in the United States, *Atmos. Environ.*, *41*, 7389–7400.

Prospero, J. M. (1999), Long-term measurments of the transport of African mineral dust to the southeastern United States: implications for regional air quality, *J. Geophys. Res.*, *104*(D13), 15,917–15,928.

Remer, L. A., et al. (2002), Validation of MODIS aerosol retrieval over ocean, *Geophys. Res. Lett.*, *29*(12), 8008, doi:10.1029/2001GL013204.

Remer, L. A., et al. (2005), The MODIS aerosol algorithm, products and validation, *J. Atmos. Sci.*, *62*, 947–973.

Remer, L. A., D. Tanre, Y. J. Kaufman, R. Levy, and S. Mattoo (2006), Algorithm for remote sensing of Tropospheric aerosol from MODIS: Collection 5, Product ID MOD04/MYD04.

Seinfeld, J. H., and S. N. Pandis (1998), *Atmospheric Chemistry and Physics*, p. 1326, New York.

Shinozuka, Y., A. D. Clarke, S. G. Howell, V. N. Kapustin, C. S. McNaughton, J. Zhou, and B. E. Anderson (2007), Aircraft profiles of aerosol microphysics and optical properties over North America: Aerosol optical depth and its association with PM2.5 and water uptake, *J. Geophys. Res.*, *112*(D12), D12S20, doi:10.1029/2006JD007918.

Singh, H. B., W. H. Brune, J. H. Crawford, D. J. Jacob, and P. B. Russell (2006), Overview of the summer 2004 Intercontinental Chemical Transport Experiment-North America (INTEX-A), *J. Geophys. Res.*, *111*(D24), D24S01, doi:10.1029/2006JD007905.

Smirnov, A., B. N. Holben, T. F. Eck, O. Dubovik, and I. Slutsker (2000), Cloud screening and quality control algorithms for the AERONET database, *Remote Sens. Environ.*, *73*, 337–349.

Spurr, R. J. D. (2002), Simultaneous radiative transfer derivation of intensities and weighting functions in a general pseudospherical treatment, *J. Quant. Spectrosc. Radiat. Transfer*, *75*, 129–175.

Sullivan, R. C., and K. A. Prather (2005), Recent advances in our understanding of atmospheric chemistry and climate made possible by on-line aerosol analysis instrumentation, *Anal. Chem.*, *77*, 3861–3886.

Sullivan, A. P., R. E. Peltier, C. A. Brock, J. A. de Gouw, J. S. Holloway, C. Warneke, A. G. Wollny, and R. J. Weber (2006), Airborne measurements of carbonaceous aerosol soluble in water over northeastern United States: Method development and an investigation into water-soluble organic carbon sources, *J. Geophys. Res.*, *111*(D23), D23S46, doi:10.1029/2006JD007072.

Thornhill, K. L., et al. (2008), The impact of local sources and long-range transport on aerosol properties over the northeast U.S. region during INTEX-NA, *J. Geophys. Res.*, *113*(D8), D08201, doi:10.1029/2007JD008666.

Turquety, S., et al. (2007), Inventory of boreal fire emissions for North America in 2004: the importance of peat burning and pyro-convective injection, *J. Geophys. Res.*, *112*(D12), D12S03, doi:10.1029/2006JD007281.

van Donkelaar, A., R. V. Martin, and R. J. Park (2006), Estimating ground-level PM 2.5 using aerosol optical depth determined from satellite remote sensing, *J. Geophys. Res.*, *111*(D21), D21201, doi:10.1029/2005JD006996.

van Donkelaar, A., R. V. Martin, R. J. Park, C. L. Heald, T. M. Fu, H. Liao, and A. Guenther (2007), Model evidence for a significant source of secondary organic aerosol from isoprene, *Atmos. Environ.*, *41*, 1267–1274.

Wang, J., and S. A. Christopher (2003), Intercomparison between satellite-derived aerosol optical thickness and PM$_{2.5}$ mass: Implication for air quality studies, *Geophys. Res. Lett.*, *30*(21), 2095, doi:10.1029/2003GL018174.

Wang, J., and S. T. Martin (2007), Satellite characterization of urban aerosols: Importance of including hygroscopicity and mixing state in the retrieval algorithms, *J. Geophys. Res.*, *112*(D17), D17203, doi:10.1029/2006JD008078.

Wang, J., D. J. Jacob, and S. T. Martin (2008), Sensitivity of sulfate direct climate forcing to the hysteresis of particle phase transitions, *J. Geophys. Res.*, *113*(D11), D11207, doi:10.1029/2007JD009368.

Weber, R. J., D. Orsini, Y. Daun, Y.-N. Lee, P. Klotz, and F. Brecktel (2001), A particle-in-liquid collector for rapid measurements of aerosol chemical composition, *Aerosol Sci. Technol.*, *35*, 718–727.

Yevich, R., and J. A. Logan (2003), An assessment of biofuel use and burning of agricultural waste in the developing world, *Global Biogeochem. Cycles*, *17*(4), 1095, doi:10.1029/2002GB001952.

Zhang, Q., D. G. Streets, K. He, and Z. Klimont (2007), Major components of China's anthropogenic primary particulate emissions, *Environ. Res. Lett.*, *2*, doi:10.1088/1748-9326/2/4/045027.

B. E. Anderson, NASA Langley Research Center, Mail Stop 483, Hampton, VA 23681, USA.

A. D. Clarke and C. McNaughton, School of Ocean and Earth Science and Technology, University of Hawaii, 1000 Pope Road, MSB 506, Honolulu, HI 96822, USA.

J. Dibb, Institute for the Study of Earth, Oceans, and Space, University of New Hampshire, Morse Hall, 39 College Road, Durham, NH 03824, USA.

E. Drury, School of Engineering and Applied Sciences, National Renewable Energy Laboratory, 1617 Cole Blvd., Golden, CO 80401-3393, USA. (easan.drury@nrel.gov)

D. J. Jacob, Department of Earth and Planetary Sciences and Division of Engineering and Applied Sciences, Harvard University, Pierce Hall, 29 Oxford Street, Cambridge, MA 02138, USA.

Y. Shinozuka, Sunphotometer Satellite Team, NASA Ames Research Center, Moffett Field, MS 245-5, Mountain View, CA 94035, USA.

R. J. D. Spurr, RT Solutions, Inc., 9 Channing Street, Cambridge, MA 02138, USA.

J. Wang, Department of Geosciences, University of Nebraska, 900 North 16th Street, 303 Bessey Hall, Lincoln, NE 68508, USA.

R. Weber, School of Earth and Atmospheric Sciences, Georgia Institute of Technology, 311 Ferst Dr. NW, Atlanta, GA 30332, USA.